

Josephson junctions as detectors for non-Gaussian noise

B. Huard^{1,*}, H. Pothier^{1,*}, Norman O. Birge^{1,**}, D. Esteve¹, X. Waintal², and J. Ankerhold³

¹ Quantronics group, Service de Physique de l'État Condensé, DRECAM, CEA-Saclay, 91191 Gif-sur-Yvette, France

² Nanoelectronics group, Service de Physique de l'État Condensé, DRECAM, CEA-Saclay, 91191 Gif-sur-Yvette, France

³ Institut für Theoretische Physik, Universität Ulm, Albert-Einstein-Allee 11, 89069 Ulm, Germany

Non-Gaussian fluctuations of the electrical current can be detected with a Josephson junction placed on-chip with the noise source. We present preliminary measurements with an NIS junction as a noise source, and a Josephson junction in the thermal escape regime as a noise detector. It is shown that the Josephson junction detects not only the average noise, which manifests itself as an increased effective temperature, but also the noise asymmetry. A theoretical description of the thermal escape of a Josephson junction in presence of noise with a non-zero third cumulant is presented, together with numerical simulations when the noise source is a tunnel junction with Poisson noise. Comparison between experiment and theory is discussed.

Copyright line will be provided by the publisher

1 Introduction

The fluctuations of the electrical current reveal the charge of the carriers, their correlations as well as their fermionic nature. Until recently, only the variance of the current fluctuations had been measured and predicted. Theoretical progress in the last decade allowed one to calculate the full counting statistics of electrons passing through any phase coherent circuit made of conductors such as tunnel junctions, quantum point contacts, diffusive wires or chaotic cavities[1, 2, 3, 4, 5]. For short enough measurement times, the distribution of the number of transmitted charges is predicted to differ sizeably from a Gaussian distribution. On the experimental side, few experiments have gone further than measuring the average noise, i.e. the quadratic average of the fluctuations. Indeed, observing a departure from the Gaussian distribution of the fluctuations requires the measurement of small signals in a short time with a high accuracy. The pioneering experiment performed by Reulet *et al.* [6] used analog microwave techniques to reconstruct $\langle V^3 \rangle$, with V the voltage across a current-biased, $\sim 50 \Omega$ -resistance tunnel junction. This first measurement of the third order cumulant of the voltage fluctuations (or skewness) pointed out the importance of feedback effects associated with the electromagnetic environment of a noise source[7, 8]. Bomze *et al.* [9] performed a direct counting of single tunneling events across a tunnel junction, using a high-precision analog-to-digital converter. Another approach consists in using an on-chip detector[10]. The statistics of the charge in quantum dots in the classical regime of sequential tunneling was probed with a quantum point contact [11, 12]. It was also shown that the current through a Josephson junction in the Coulomb blockade regime is sensitive to non-Gaussian noise [13]. A promising scheme to probe current fluctuations, proposed by Tobiska and Nazarov [14], consists in using a Josephson junction as a threshold detector. The switching of

* Corresponding author E-mail: hugues.pothier@cea.fr

** Permanent address: Department of Physics and Astronomy, Michigan State University, East Lansing, Michigan 48824-2320, USA

a Josephson junction out of the zero-voltage state provides a sensitive threshold detector because the switching rate varies exponentially with the bias current. We present here a preliminary experiment in which a current-biased Josephson junction is capacitively coupled to a voltage-biased tunnel junction which induces current fluctuations in the Josephson junction. A similar experiment was performed by Timofeev *et al.* [15] using a junction in a regime involving macroscopic quantum tunneling, thermal escape and phase diffusion. The response of the Josephson junction to the squewness of current fluctuations was compared with an adiabatic model which uses as an input the measured response to the average current and as a fit parameter a bandwidth, of the order of the plasma frequency. In our experiment, the junction is kept in the regime of thermal escape which allows direct comparison to theory. The switching rate of the Josephson junction is measured for opposite values of the average bias current I_b through it, thus giving access to the asymmetry of the current fluctuations. In a second part, theoretical predictions for the response of the Josephson junction to fluctuations with a non-zero third cumulant are presented, under the assumption that the correlation time of the fluctuations is shorter than the response time of the Josephson junction, and that feedback effects related to the voltage developing on the Josephson junction can be neglected. The results of this calculation are then compared with numerical simulations that integrate the Langevin equation describing the phase dynamics in presence of current fluctuations created by uncorrelated tunnel events. Finally, experimental results are confronted with theory.

2 Measuring noise with a Josephson junction

In a simplistic picture, a Josephson junction biased at an average current I_b below its critical current I_0 can be seen as a threshold detector for current fluctuations: neglecting thermal activation or quantum tunneling, the junction remains in its zero-voltage state as long as the current fluctuations are smaller than $I_0 - I_b$. When the current exceeds this limit, the junction switches to the dissipative state, and a voltage develops. This voltage subsists until a “reset” is performed,

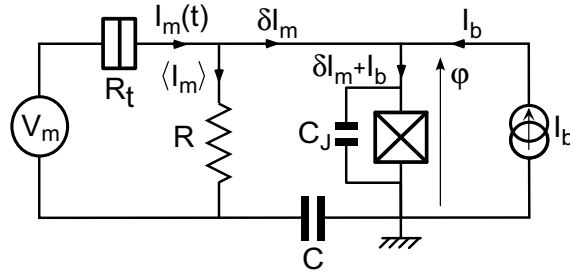


Fig. 1 Simplified scheme of the experiment. The high frequency ($f > 1/RC$) fluctuations δI_m of the current through a voltage-biased tunnel junction pass through a Josephson junction. The switching of the Josephson junction to the finite-voltage state depends on the sum of δI_m and of the pulsed current bias $I_b(t)$. The switching probability of the junction during one pulse can be related to the current fluctuations.

by driving the bias current down to zero, then back to I_b . The behavior of the Josephson junction is thus similar to that of an electrical circuit breaker. The principle of our experiment is to couple, through a capacitor, the current fluctuations δI_m of a voltage-biased noise source to a current-biased Josephson junction (see Fig. 1), and to compare the switching rates Γ_+ and Γ_- at opposite values of the bias current $\pm I_b$ applied during a time τ_p through the Josephson junction. The asymmetry in the rates $R_\Gamma = \Gamma_+/\Gamma_- - 1$ reflects the difference in the probabilities that during τ_p

fluctuations such that $\delta I_m > I_0 - I_b$ and $\delta I_m < -(I_0 - I_b)$ occur, *i.e.* the asymmetry in current fluctuations whose amplitude exceeds $I_0 - I_b$.

However, a Josephson junction is not a perfect threshold detector: the switching of a Josephson junction occurs for bias currents I_b smaller than I_0 , because of thermal activation or quantum tunneling. As explained below, thermal activation is the dominant process in our experiment; we will thus consider this case only. Any dissipative impedance connected to the Josephson junction produces Johnson-Nyquist current noise, which can yield thermal escape and switching. The theoretical description of this phenomenon is based on the Resistively Shunted Junction (RSJ) model, in which the dynamics of the Josephson junction is similar to that of a particle in a tilted washboard potential with friction [16, 17]. The state of the Josephson junction is characterized by the phase difference φ across the junction, which relates to the position of the fictitious particle. The particle evolves in the Josephson potential $-E_J(\cos \varphi + s\varphi)$, where $E_J = I_0\varphi_0$ is the Josephson energy, with $\varphi_0 = \hbar/2e$, and $s = I_b/I_0$ the reduced bias current, which determines the average slope of the potential. At small bias current, the particle is trapped in a local minimum and oscillates at the plasma frequency $\omega_p(s) = \omega_0(1 - s^2)^{1/4}$, where the frequency $\omega_0 \simeq (I_0/\varphi_0 C_J)^{1/2}$ is set by the parallel capacitance C_J . When the current increases further, the thermal energy can become comparable to the barrier height $\Delta U(s) \approx (4\sqrt{2}/3)\varphi_0 I_0(1 - s)^{3/2}$. The particle can then be thermally activated over the barrier and escape from the local minimum at a rate

$$\Gamma(s) \simeq \underbrace{\frac{\omega_p(s)}{2\pi}}_A \underbrace{e^{-\Delta U(s)/k_B T_{\text{esc}}}}_{e^{-B}} \quad (1)$$

In this expression, the escape temperature T_{esc} is a measure of the current noise in the circuit connected to the Josephson junction, mostly at the plasma frequency. In the setup presented in Fig. 1, two noise sources are connected to the Josephson junction: the resistance R in series with the tunnel junction, that can be assumed to be at the bath temperature T_0 , and the tunnel junction itself, whose current noise is described by a spectral density $2e \langle I_m \rangle \coth(eR_t \langle I_m \rangle / 2k_B T_0)$, with R_t the tunnel resistance. In a simple model, the escape temperature in Eq. (1) is therefore given by [18]:

$$T_{\text{esc}} = (1/R + 1/R_t)^{-1} (T_0/R + e \langle I_m \rangle / 2k_B \coth(eR_t \langle I_m \rangle / 2k_B T_0)). \quad (2)$$

In this setup, the Josephson junction is thus very sensitive to the second moment of the current fluctuations [19, 20].

The measurements presented here were obtained on a sample with an aluminum Josephson junction of area $0.7 \mu\text{m}^2$, in parallel with a capacitor $C_J = 36 \text{ pF}$. For convenience in sample fabrication, the noise source under investigation was not a normal (NIN) tunnel junction, but a $0.2 \mu\text{m}^2$ NIS junction made of Al and Cu electrodes separated by a tunnel barrier obtained simultaneously with the barrier of the Josephson junction by oxidation of the aluminum layer. In order for the electromagnetic environment of the Josephson junction to be entirely determined by on-chip elements, large capacitors ($C_1 \approx 850 \text{ pF}$ and $C \approx C_2 \approx 130 \text{ pF}$) were fabricated on-chip between the connecting pads and ground (see Fig. 2). These capacitors and the junction capacitor C_J were made using plasma oxidized aluminum electrodes deposited on the substrate prior to patterning the circuit [18]. At frequencies of the order of the plasma frequency, the capacitors act as short circuits in parallel with the circuit placed outside the chip. Capacitance C_1 also allows for a good voltage bias of the junction and reduces the low-frequency cut-off of the high-pass filter associated with R_f and C . Resistors $R_f = 202 \Omega$ and $R_b = 202 \Omega$ were commercial surface mount NiCr resistors connected directly on the sample with silver epoxy. The sample holder was thermally anchored to the mixing chamber of a dilution refrigerator with a base temperature of 20 mK. All lines connected to the sample were twisted pairs equipped with microwave filters, except a 50Ω coaxial line with distributed 50 dB attenuation designed to apply

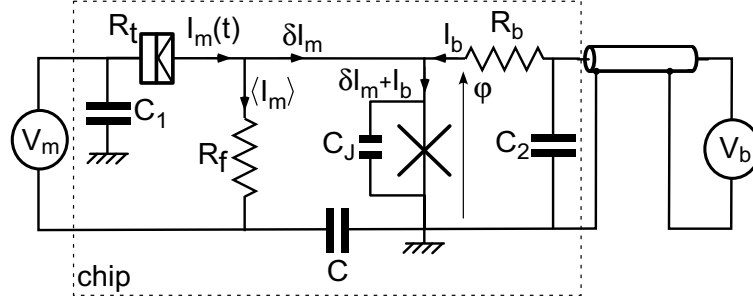


Fig. 2 Full scheme of the experiment. The noise source is a Cu-Al NIS tunnel junction. The current pulses through the Josephson junction are obtained by voltage pulses on a coaxial line, applied to the series combination of a bias resistor R_b and the Josephson junction. Large capacitors C , C_1 and C_2 allow for good voltage bias and limit the impedance seen by the Josephson junction to on-chip elements.

current pulses to the Josephson junction. The floating bias of the NIS tunnel junction was realized with a battery-operated voltage divider, followed by an electrical two-position switch that allowed reversals of the sign of the bias (at ~ 1 Hz) to eliminate the effect of drifts. Bias resistors of $10\text{ M}\Omega$ were placed on the two wires of the twisted pair connecting the voltage source to the samples. The voltage was measured across the series combination of the tunnel junction (noise source) and of the Josephson junction (detector), allowing for measurements of one or the other, depending on the bias scheme. For example, the $I - V$ characteristics of the NIS junction shown in Fig. 3 was measured with $I_b = 0$, so that the voltage drop across the Josephson junction was zero. From this characteristic taken at 20 mK , we deduced the tunnel resistance $R_t = 1.57\text{ k}\Omega$. In the following, we describe measurements with the NIS junction biased above the gap voltage, in a transport regime dominated by tunneling of single electrons, like in a usual NIN tunnel junction.

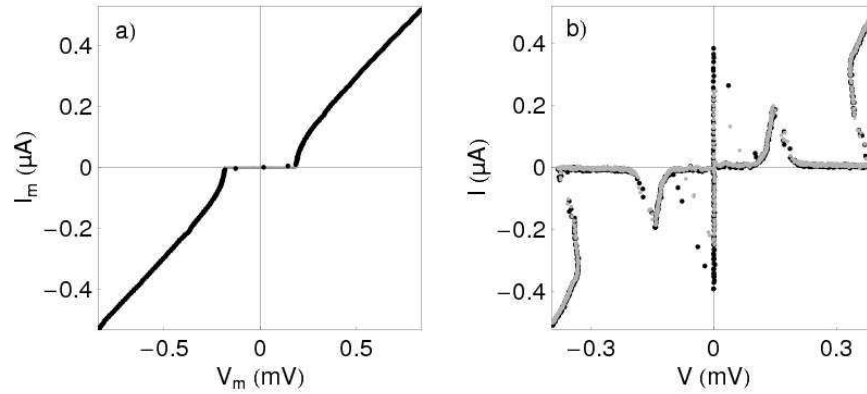


Fig. 3 a) Current-voltage characteristics of the NIS junction at a refrigerator temperature of $T_0 = 20\text{ mK}$. A fit to theory yields the tunnel resistance of $R_t = 1.57\text{ k}\Omega$ and the superconducting gap $\Delta = 185.5\text{ }\mu\text{eV}$. b) Current-voltage characteristics of the Josephson junction at two different values of the current I_m in the NIS junction and at a refrigerator temperature of $T_0 = 20\text{ mK}$. The black dots were measured with $\langle I_m \rangle = 5.3\text{ nA}$ and the grey dots with $\langle I_m \rangle = 640\text{ nA}$.

The current-voltage characteristics of the Josephson junction, shown in Fig. 3 for two values of the current through the NIS junction, is obtained by sweeping back and forth the voltage V_b , and recording both the current (from the voltage across a $10\,\Omega$ resistor placed at the base temperature) and the voltage. A supercurrent branch is observed, and when V_b/R_b exceeds a threshold I_{sw} , the junction switches. The current then drops essentially to zero, with the applied voltage $V_b = R_b I_{sw} \sim 0.1\,\text{mV} < 2\Delta/e$ now entirely across the Josephson junction. Compared to a perfect current bias, our bias scheme limits the production of quasiparticles at the Josephson junction. However, we observed in the $I - V$ characteristics of the Josephson junction a large sub-gap current peak close to $V \sim 0.15\,\text{mV}$, leading to increased heating for the largest switching current. We therefore had to reduce the duty cycle of the applied pulses to a value such that heating could be neglected. In order to extract the parameters determining the dynamics of the Josephson junction, we first used resonant activation [21, 18] to extract the plasma frequency $\omega_0 \simeq 1.0\,\text{GHz}$ at $s = 0$, and determine its quality factor $Q_0 \simeq 22$. In addition, from the value of the plasma frequency, one can estimate the cross-over temperature between the regimes of thermal activation and quantum tunneling: $T_{co} = \hbar\omega_p/2\pi k_B \approx 8\,\text{mK} \ll T_0$. Therefore, and as stated above, switching does occur due to thermal activation for all experimentally accessible temperatures. Then, from the measurement of the number of switching events for a large number of current pulses, we deduced the dependence of the switching rate on the current through the Josephson junction. Equation (1) then yields the critical current $I_0 \simeq 0.48\,\mu\text{A}$ and the escape temperature $T_{esc} \simeq 35\,\text{mK}$. The fact that the latter temperature is slightly larger than the fridge temperature comes mainly from the heating of the resistor R_b by the current pulses [18].

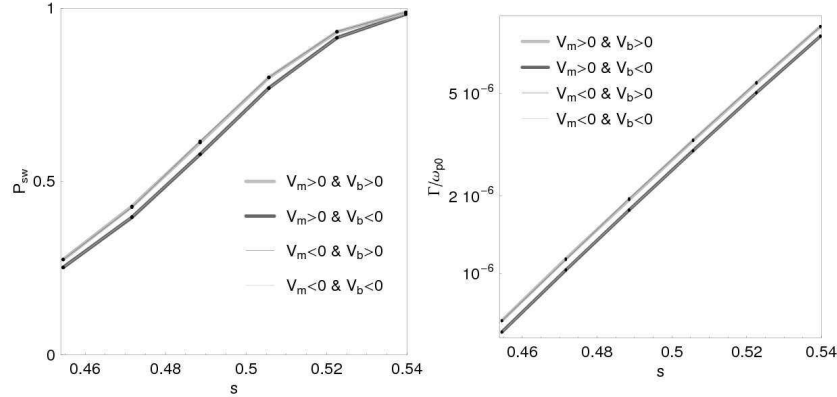


Fig. 4 Switching probability P_{sw} (left panel) and corresponding switching rates Γ (right panel) as a function of the reduced pulse height $s = I_b/I_0$ for $\langle I_m \rangle \approx 1.1\,\mu\text{A}$ at a temperature $T_0 \approx 197\,\text{mK}$. The probabilities are calculated from statistics on 2×10^5 to 5×10^5 pulses in order to achieve a constant relative uncertainty $5 \times 10^{-8}\omega_0$ on the rate Γ (see Appendix), smaller than the size of the dots. The four curves correspond to four combinations of the signs of V_m and V_b . Pairs with identical sign of $V_m \times V_b$ are almost superimposed, as expected from time-reversal symmetry.

For non-zero values of the average current $\langle I_m \rangle$ through the NIS junction, where the statistics of tunneling events are expected to be Poissonian, the switching properties of the Josephson junction are probed as follows. Sequences of 10^4 current pulses with alternating polarity and of duration $\tau_p \approx 50\,\mu\text{s}$ are applied to the Josephson junction. In order to circumvent artifacts associated with possible DC offsets and thermoelectric effects, the current pulses are sent through a large, room temperature capacitor ($200\,\mu\text{F}$). For each pulse, the voltage across the Josephson junction

is monitored by two threshold detectors, each detecting the switching events in one of the two current directions (appearance of a positive or a negative voltage larger than a fixed threshold). Between each sequence of 10^4 pulses, the polarity of the current $\langle I_m \rangle$ through the NIS junction is inverted. The switching probabilities P_{sw} can then be reconstructed for 4 combinations of the signs of I_m and I_b . It was carefully checked that the combinations $(I_m > 0, I_b > 0)$ and $(I_m < 0, I_b < 0)$, on the one hand, and $(I_m > 0, I_b < 0)$ and $(I_m < 0, I_b > 0)$, on the other hand, give the same results, as expected from symmetry considerations. As an example, the dependence of P_{sw} on $s = |I_b|/I_0$ is shown in Fig. 4 for $\langle I_m \rangle = \pm 1.1 \mu\text{A}$.

This measurement is then repeated for various pulse heights, and for various I_m . The range of pulse heights was chosen to keep the relative uncertainty on the switching rates small (see appendix). Information on the average noise and its asymmetry are extracted from these data. We first focus on the average noise, which is the largest effect, seen in the escape temperature T_{esc} according to Eq. (1).

From P_{sw} , one extracts the switching rate $\Gamma = -\tau_p^{-1} \log(1 - P_{sw})$ and the curve $\Gamma(s)$ is fitted with Eq. (1). The only fitting parameter is the escape temperature T_{esc} , which does not change for opposite current directions within the experimental error margins. The dependence of T_{esc} on $\langle I_m \rangle$ is shown in Fig. 5, for bath temperatures T_0 from 20 mK to 530 mK.

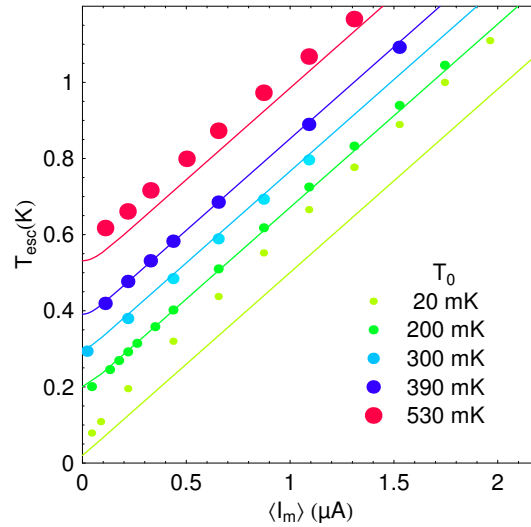


Fig. 5 Escape temperatures extracted using Eq. 1 (with $I_0 = 479 \text{ nA}$, $C = 36 \text{ pF}$) from the measurement of the rate as a function of s for several values of the current in the tunnel junction I_m and of the refrigerator temperature T_0 . The lines show the behavior expected from Eq.(3), in which $a = eR_{\parallel}/2k_B$ was taken as a fit parameter ($a_{\text{fit}} \simeq 0.48 \text{ K}/\mu\text{A}$).

Apart from the 20 mK data, one finds (lines in Fig. 5) $T_{\text{esc}} \simeq 0.95 T_0 + a \langle I_m \rangle$, with $a \simeq 0.48 \text{ K}/\mu\text{A}$. This slope can be compared to the prediction (2), in which R has to be replaced with the parallel combination of R_f and R_b : at $eR_{\parallel} \langle I_m \rangle \gg 2k_B T_0$, one expects

$$\begin{aligned} T_{\text{esc}} &= R_{\parallel} (1/R_f + 1/R_b) T_0 + eR_{\parallel} \langle I_m \rangle / 2k_B \coth [eR_{\parallel} \langle I_m \rangle / 2k_B T_0] \\ &\approx 0.95 T_0 + eR_{\parallel} \langle I_m \rangle / 2k_B, \end{aligned} \quad (3)$$

with $R_{\parallel} = (1/R_f + 1/R_b + 1/R_t)^{-1}$, leading to $a \simeq 0.55 \text{ K}/\mu\text{A}$, in reasonable agreement with the value observed. The slight difference in a can be attributed to an imperfect modeling of the impedance seen by the Josephson junction near $\omega_p/2\pi \approx 1 \text{ GHz}$, where it is the most sensitive.

The increased escape temperature at $T_0 = 20$ mK is well explained by electron heating in the resistors R_f and R_b in presence of the currents I_m and I_b [18, 22].

The switching of a Josephson junction is not only sensitive to the average noise power of current fluctuations, but also to higher order cumulants. The contribution of the cumulants with odd order yield an asymmetry of the switching rate $R_\Gamma(s) = \Gamma_+(s)/\Gamma_-(s) - 1$, with $\Gamma_+(s)$ the rate when I_b and I_m have the same sign, $\Gamma_-(s)$ when they have opposite signs. As discussed in the appendix, we acquired data only for a $0.25 < P_{sw} < 0.987$, an interval in which a good precision on R_Γ can be reached with achievable numbers N of measurement pulses. Since T_{esc} increases with $\langle I_m \rangle$, data taken at various $\langle I_m \rangle$ correspond to different ranges of s . For example, at 20 mK, $s \approx 0.9$ at $\langle I_m \rangle = 0.04 \mu\text{A}$ and $s \approx 0.3$ at $\langle I_m \rangle = 2 \mu\text{A}$. This limits the accessible range for the current I_m .

The existence of an asymmetry can be seen already in the raw data (Fig. 4). Figure 6 shows, for various temperatures T_0 , the dependence of the asymmetry R_Γ on $\langle I_m \rangle$ for the two extreme values of rate exponents $B = 9.5$ and $B = 11.5$, corresponding to $P_{sw} \approx 0.25$ and $P_{sw} \approx 0.987$, and to switching rates $\Gamma \approx 6$ kHz and $\Gamma \approx 90$ kHz. In each case, the two curves are very similar, with R_Γ increasing continuously with $\langle I_m \rangle$.

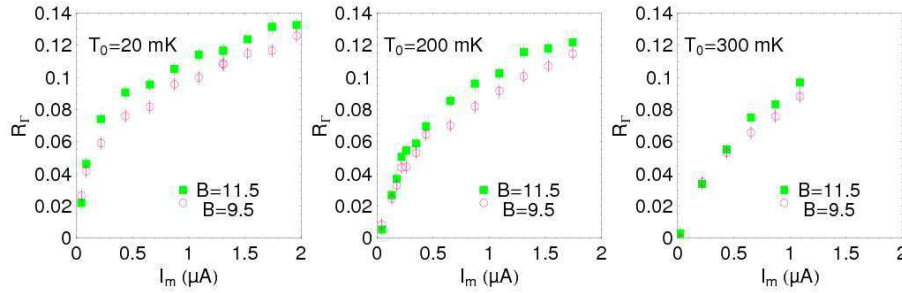


Fig. 6 Measured asymmetry R_Γ between positive and negative bias schemes as a function of the mean current I_m through the tunnel junction. Each panel corresponds to a single refrigerator temperature T_0 and each symbol corresponds to a fixed value of the rate exponent B from Eq. (1). Error bars are shown as lines (see Appendix).

In order to compare these results with theory, we first discuss how the switching of a Josephson junction is affected by non-gaussian white noise.

3 Dynamics of a Josephson junction in presence of non-Gaussian noise

In this section we present a theoretical analysis of the switching of a Josephson junction out of its zero voltage state driven by thermal as well as weak non-Gaussian noise. According to the experimental situation described above (Fig. 1), the underlying stochastic processes are assumed to be classical, both for the dynamics of the detector, the Josephson junction, and for the electrical noise originating from the mesoscopic conductor, the tunnel junction. Hence, the standard RSJ model applies, where now the total noise consists of the Johnson-Nyquist noise δI , in the simplest case produced by a resistor R in parallel to the Josephson junction, and of the mesoscopic noise δI_m from the fluctuating part of the mesoscopic current $I_m = \langle I_m \rangle + \delta I_m$. Since the dc-component $\langle I_m \rangle$ of the mesoscopic current can be incorporated trivially, we only focus in the sequel on its fluctuating part δI_m . Then, according to the Kirchhoff rules we have for the currents entering the detector

$$I_b + \delta I_m(t) = \frac{V}{R} + I_0 \sin \varphi + C_J \dot{V}, \quad (4)$$

where φ denotes its phase difference and the other quantities are defined according to Fig. 1. To proceed it is convenient to work with dimensionless quantities and to scale times with ω_0 , energies with E_J , and currents with I_0 . This way, we arrive with $\dot{\varphi} = V/\varphi_0$ and $\tau = \omega_0 t$, at a classical Langevin equation for the phase dynamics, i.e.,

$$\ddot{\varphi} = -\sin \varphi - \frac{\dot{\varphi}}{Q_0} + s_b + s_m(\tau) + s_{th}(\tau) \quad (5)$$

with the quality factor $Q_0 = RC_J\omega_0$ of the unbiased junction, the scaled bias current $s_b = I_b/I_0$, and the scaled noise sources $s_{th} = \delta I/I_0$ and $s_m = \delta I_m/I_0$ for thermal and non-Gaussian noise, respectively. These two noisy forces are assumed to be Markovian, which is an accurate approximation since the experiment is operated in a regime where the typical correlation times are much smaller than the typical time scales of the junction, e.g. the inverse of the plasma frequency. This situation also ensures that we can work with continuous noise processes. Hence, we have for the thermal noise $\langle s_{th} \rangle = 0$ and

$$\langle s_{th}(\tau)s_{th}(0) \rangle = \frac{2\theta}{Q_0} \delta(\tau), \quad (6)$$

where we introduced the dimensional temperature $\theta = k_B T_0/E_J$. The non-Gaussian noise produced by the tunnel junction is taken as Poissonian with $\langle s_m \rangle = 0$, where specifically the second moment reads in the high voltage/low temperature limit ($eR_t I_m \gg 2k_B T_0$)

$$\langle s_m(\tau)s_m(0) \rangle = F_2 \alpha^2 \Lambda_m \delta(\tau), \quad (7)$$

with $\Lambda_m = \langle I_m \rangle/I_0 \alpha$, $\alpha = e\omega_0/I_0$ and the third moment is given by

$$\langle s_m(\tau_2)s_m(\tau_1)s_m(0) \rangle = F_3 \alpha^3 \Lambda_m \delta(\tau_2)\delta(\tau_1). \quad (8)$$

The prefactors F_2 and F_3 are the Fano factors for the second and third cumulant. Here, for the tunnel junction, $F_2 = F_3 = 1$. It is important to realize that the average mesoscopic current Λ_m can be large so that the second moment (7) can be comparable to or larger than that of the thermal noise (6), while the third moment is still small due to $\alpha \ll 1$. In fact, as discussed above, the Gaussian component of the mesoscopic noise effectively adds to the thermal noise to determine the effective temperature of the junction

$$\begin{aligned} \theta_{\text{eff}} &= \theta + \theta_m \\ &\equiv \theta + F_2 \frac{\alpha^2 \Lambda_m Q_0}{2}. \end{aligned} \quad (9)$$

So far we have assumed that the resistance seen by the Josephson junction is exclusively given by the resistance R in parallel to it so that (9) agrees with (2) only in the limit $R_t \gg R$. In a description closer to the experimental situation the total resistance is $RR_t/(R + R_t)$ and we have to replace $\theta_{\text{eff}} \rightarrow R_t/(R + R_t) \theta_{\text{eff}}$, thus arriving precisely at (2). Another simplification is that in the Langevin equation (5) no back-action effect from the detector to the tunnel junction has been taken into account. The back-action appears because when the Josephson junction switches, the voltage across the tunnel junction no longer coincides with the external voltage, but is reduced by $(\hbar/2e)\langle \dot{\varphi} \rangle$. Accordingly, on the one hand in the friction term in (5) Q_0 has to be replaced by $R_t/(R + R_t)Q_0$ and on the other hand the third moment (8) carries for finite eV/θ_{eff} an additional contribution from the derivative of the second moment (7) with respect to the voltage. For a detailed quantitative comparison with the experiment these modifications must be taken into account.

Based on (5) we first give a brief account of a theoretical approach developed recently by one of us [23], where an analytical expression for the rate and its asymmetry due to a weak third cumulant of a current through a mesoscopic conductor has been derived. In a second part, direct numerical simulations are presented, which allow for a detailed comparison with the analytical predictions and may thus lay out a firm basis for the comparison between theory and experiment.

3.1 Analytical rate expression

As usual in rate theory, for analytical treatments it is much more convenient to work with phase space probabilities rather than individual stochastic trajectories. The general problem for non-Gaussian noise is then that the corresponding Fokker-Planck equation (FPE) based on a Kramers-Moyal expansion contains diffusion coefficients up to infinite order. The basic idea for weak non-Gaussian noise with a leading third cumulant is thus to derive an effective, finite order Fokker-Planck equation. Based on a cumulant expansion of the noise generating functional such a generalized FPE has been derived in [23] and leads to a FPE with a momentum dependent diffusion term, where the momentum dependence is weighted by the third cumulant.

The existence of a time-independent switching rate is associated with a quasi-stationary nonequilibrium distribution, which reduces to a thermal equilibrium in the well region and deviates from it only around the barrier top in the case where friction is moderate to high. This in turn means that the barrier height compared to the thermal energy must be sufficiently large $\Delta U/k_B T_{\text{eff}} \gg 1$ so that switching becomes a rare event on the time scale of the plasma frequency. The typical thermal rate expression then looks as in (1) and is dominated by the exponential (activation factor) being identical to the probability to reach the barrier top from the well bottom by a thermal fluctuation. Accordingly, the quasi-stationary state (the flux state) is written as a product consisting of the thermal distribution and a 'form factor' describing the deviation from it around the barrier top. The latter one leads to the rate prefactor, while the former one specifies the activation factor. Here, we restrict ourselves to the exponential factor, which provides by far the dominant contribution in the present experimental set-up. Within this theoretical framework in [23] an analytical expression for the exponent including leading corrections due to a third cumulant have been obtained. The rate takes the form $\Gamma_{\pm} \propto \exp[-B(1 \mp |g|)]$ with the dimensionless barrier height $B = \Delta U/(E_J \theta_{\text{eff}})$ and the correction g due to the third cumulant such that Γ_+ corresponds to $\Lambda_m > 0$ and Γ_- to $\Lambda_m < 0$. Note that we thus consider the bias current s_b as being always positive, while the situation in which one keeps $\Lambda_m > 0$ and inverts the bias current follows straightforwardly.

In the dimensionless quantities introduced above one has

$$B = \frac{4\sqrt{2}}{3\theta_{\text{eff}}}(1 - s_b)^{3/2}. \quad (10)$$

The rate asymmetry $R_{\Gamma} = \Gamma_+/\Gamma_- - 1$ is found as [24]

$$R_{\Gamma} \approx \exp \left[F_3 \frac{16\sqrt{2}\alpha^3 |\Lambda_m|}{9\theta_{\text{eff}}^3} \frac{Q^2}{5 + Q^2} \frac{(1 - s_b)^{5/2}}{\sqrt{1 - s_b^2}} \right] - 1 \quad (11)$$

with the quality factor of the biased junction $Q = Q_0(1 - s_b^2)^{1/4}$. For weak friction $Q \gg 1$, the only dependence of R_{Γ} on friction is through the effective temperature (see Eq. (9)). When the asymmetry is small enough, it is directly proportional to the Fano factor F_3 , leading to a clear measure of the third order cumulant of the noise (Fig. 7b).

Let us first look at the dependence of R_{Γ} when the mesoscopic current varies (Fig. 7a). For small Λ_m the effective temperature coincides with the actual temperature $\theta_{\text{eff}} \approx \theta$ and R_{Γ} grows linearly with Λ_m . For large Λ_m the heating originates solely from the mesoscopic current, i.e. $\theta_{\text{eff}} \approx \theta_m \propto \Lambda_m$, so that R_{Γ} decreases roughly $\propto 1/\Lambda_m^2$ and the rate asymmetry vanishes due to a growing second cumulant compared to the third one. Consequently, there is a changeover between these two regimes with a maximum of the rate asymmetry around the range, where $\theta \approx \theta_m = \alpha^2 \Lambda_m Q_0/2$ [see (9)].

In the experiment, the junction is operated essentially at a fixed switching rate, with s_b tuned at each mesoscopic current Λ_m to a value such that B is kept constant. In this situation it is instructive to look for the scaling properties of the rate asymmetry as a function of the bare

exponent B . In general, to express $R_{\Gamma}(s_b)$ in terms of B leads to a rather involved expression. Transparent formulae are found if the asymmetry is sufficiently small so that a linearization of the exponential in (11) applies, for vanishing thermal noise $\theta = 0$, and in the limits of strong and weak friction, respectively. Then, one writes for (11) $R_{\Gamma}(B) \approx \xi_{\eta} B^{\eta}$ and looks for that exponent η for which the prefactor ξ_{η} displays the weakest dependence on B . This way, one finds in the regime of weak friction that $\eta \approx 1.45$, while for strong friction one has $\eta \approx 5/3$.

To complete this discussion, we remark that an analytical expression for the asymmetry of the escape rate in the limits of low and high friction has been also derived in [25] within the framework of an Onsager-Machlup type of functional representation of the stochastic process combined with an asymptotic evaluation (high barrier, weak third cumulant) of the path integrals. The expression (11) reduces for low Q exactly to the one specified there. For high Q both results give also precisely the same dependence on the physical quantities, but with slightly different numerical constants. Further, back-action effects according to the discussion at the end of the previous section can be included in (11) in the same way as in Ref. [25] since both theoretical approaches start from the same Langevin equation. Hence, we conclude that, up to small corrections, both theories make identical predictions, where the advantage of (11) is that it provides an analytical expression for all damping strengths.

3.2 Numerical simulations

Direct numerical simulations of the escape rate of a Josephson junction in presence of a weakly non-Gaussian noise are based on the Langevin equation (5) with the mesoscopic noise term $s_m(t)$ being represented as

$$s_m(\tau) = \sum_i \alpha \delta(\tau - \tau_i) - \alpha \Lambda_m. \quad (12)$$

The random variables τ_i are the times at which a tunneling event occurs in the mesoscopic tunneling junction. Those tunneling events correspond to a Poisson process so that the intervals between two consecutive events $S_i = \tau_{i+1} - \tau_i$ are independently distributed according to $p(S_i) = \Lambda_m e^{-\Lambda_m S_i}$.

The numerical integration of Eq.(5) should be performed with some care as the non-Gaussian effects we are looking for are rather weak. We have therefore used two independent schemes and checked for several cases that they produced identical results within statistical errors.

3.2.1 First scheme

The first scheme is a first order direct integration of the equation of motion. We discretize the time into steps of size h . Noting $\varphi_i = \varphi(\tau = ih)$ and $p_i = \dot{\varphi}(\tau = ih)$, we have

$$\begin{aligned} p_{i+1} - p_i &= (F_i - p_i/Q_0)h + \Sigma_i^m + \Sigma_i^{\text{th}} \\ \varphi_{i+1} - \varphi_i &= p_i h \end{aligned} \quad (13)$$

with

$$F_i = -\sin \varphi_i + s \quad \text{and} \quad \Sigma_i^{\Upsilon} = \int_{ih}^{(i+1)h} d\tau \, s_{\Upsilon}(\tau) \quad (\Upsilon = m; \text{th})$$

The variables Σ_i^{th} are independent and Gaussian of variance $2\theta/(Q_0 h)$. In this first scheme, we have directly sampled the variables S_i through $S_i = -\log(X_i/\Lambda_m)$ where X_i is a random number uniformly distributed within $[0, 1]$. $\Sigma_i^m = \alpha \hat{N} - \alpha \Lambda_m$ counts the number \hat{N} of tunneling events in the window $[ih, (i+1)h]$.

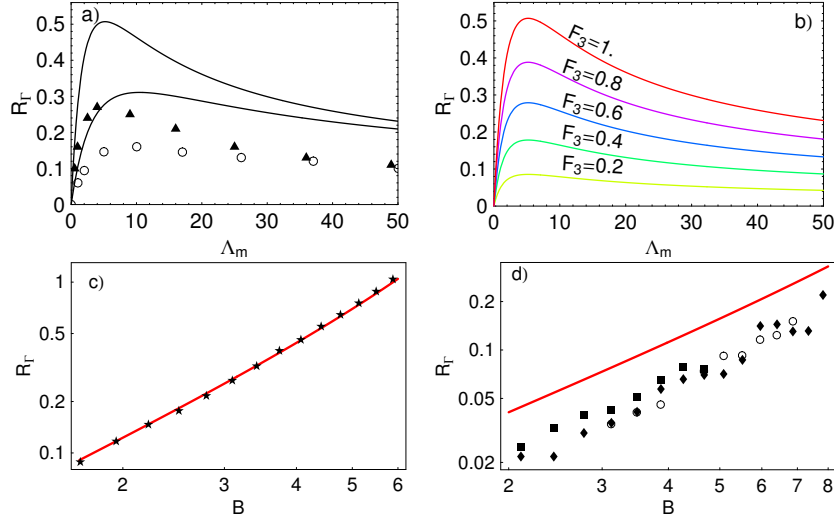


Fig. 7 Numerical results versus theory. **a)** numerical simulations for the asymmetry of the tunneling rates as a function of the current Λ_m at a fixed value of the exponent $B = 6$ in the rate (1) and for two values of the temperature $\theta = 0.005$ (\blacktriangle) and $\theta = 0.01$ (\circ). $Q_0 = 8$, $\alpha = 0.02$. The maximum occurs at the crossover $\theta_m = \theta$. The lines are plotted using Eq. (11) with the same parameters. **b)** The lines are plotted using Eq. (11) with the same parameters as in **a)** and $\theta = 0.005$. Each line corresponds to a different Fano factor for the third order cumulant of the noise. The experiment and all the other figures describe the case $F_3 = 1$. **c)** asymmetry as a function of the exponent B for $Q_0 = 0.5$, $\alpha = 0.1$, $\theta = 0$ and $\Lambda_m = 40$. The line is plotted using Eq. (11) with the same parameters. **d)** asymmetry as a function of the exponent B for $Q_0 = 10$, $\alpha = 0.02$, $\theta = 0$ and $\Lambda_m = 40$. The various symbols stand for the first integration scheme (\circ : $N = 10^5$, $h = 0.006$) and second integration scheme (\blacksquare : $N = 10^6$, $h = 0.08$; \blacklozenge : $N = 10^5$, $h = 0.0044$). The line is plotted using Eq. (11) with the same parameters.

3.2.2 Second scheme

The second scheme is a direct extension of Ref. [26] and is valid up to second order in h ,

$$\begin{aligned} p_{i+1} - p_i &= (F_i + F_{i+1})h/2 + \Sigma_i^m + \Sigma_i^{th} - (\varphi_{i+1} - \varphi_i)/Q_0 \\ \varphi_{i+1} - \varphi_i &= p_i h [1 - h/(2Q_0)] + F_i h^2/2 + (\Sigma_i^m + \Sigma_i^{th})h/2. \end{aligned} \quad (14)$$

There, we have directly sampled the number \hat{N} of tunneling events which is distributed according to $P(\hat{N} = i) = e^{-\Lambda_m h} \frac{(\Lambda_m h)^i}{i!}$.

3.2.3 Numerical results

To compute the escape rate Γ , we integrate the equations of motions N times (typically $N = 10^5$) and save the time τ_j where φ escapes its well (taken as $|\varphi| > 3.5$). We checked that the τ_j are distributed according to an exponential law $P(\tau_j < \tau) = 1 - e^{-\Gamma\tau}$. Noting τ_p the maximal time of one simulation, and $\langle n \rangle \approx e^{-\Gamma\tau_p}$ the measured probability of non switching, our estimator for Γ is $\frac{1}{\Gamma} = \frac{\langle \tau_j \rangle}{1 - \langle n \rangle}$. The asymmetry of the escape rate is defined as $R_\Gamma = \Gamma(\Lambda_m)/\Gamma(-\Lambda_m) - 1$.

For the discussion of our numerical findings let us start with a comparison with the analytical predictions presented in the previous section. In Fig.7a the rate asymmetry as a function of the average mesoscopic current Λ_m is depicted for fixed barrier height $B = 6$. In accordance

with theory R_f shows a non-monotonous behavior with a maximum around that value of Λ_m where $\theta \approx \theta_m$. For higher thermal noise the rate asymmetry shrinks for lower Λ_m , but becomes independent of thermal noise in the decreasing tail for higher Λ_m . Apparently, while the analytical expression provides the overall tendency correctly, there are quantitative deviations from the simulated data. The reason for that will be discussed below.

The scaling of the rate asymmetry as a function of B is shown in Fig.7c for strong ($Q_0 = 0.5$) and in Fig.7d for weaker ($Q_0 = 10$) friction. In the former case we find an accurate agreement with the analytical expression (11) even for low barriers. In the latter situation the analytical expression describes the scaling with respect to B correctly, however, for lower barriers the absolute values exceed the numerical ones by about 100%, while for somewhat higher barriers, for which convergent data could be obtained for $6 < B \leq 8$, the deviations become smaller, namely 50%. Note, that for weaker damping the variance of the numerical data around an average behavior increases and is typically of the order of 10%. For even larger values of B the switching becomes an extremely rare event and the statistics deteriorate drastically. The obvious discrepancy for lower barriers that has already been seen in Fig.7a does not come as a surprise since, as known from standard Kramers' rate theory, escape rates are calculated as expansions in $1/B$ and the exponential activation factor dominates only for sufficiently large B . In particular in the weak friction regime finite barrier corrections as well as the rate *prefactor* tend to play an even more important role when one approaches the energy-diffusion limit, where the rate vanishes with decreasing friction strength. The turnover between energy-diffusion and spatial-diffusion occurs around $Q_0 \approx B$ so that the simulated data displayed in Fig.7d in the range of lower barrier heights are certainly influenced by these effects.

The overall picture emerging is hence that within the statistical uncertainties of the simulations, the analytical theories developed for the switching of the Josephson junction predict quantitatively the influence of a weak third cumulant of non-Gaussian noise up to minor deviations due to prefactor effects over a broad range of parameters. As expected, larger discrepancies occur for weaker friction and lower barriers, a range beyond the strict applicability of the analytical treatments.

4 Discussion

Figure 8 presents a comparison between the measured and the predicted asymmetry in the switching rates of the Josephson junction in presence of a current in the tunnel junction. The data of the left pannel (a) correspond to the intermediate the switching exponent $B = 10.5$. The right panel (b) shows the theoretical predictions Eq. (11) for the same parameters, and assuming that the temperature is T_0 . The disagreement is significant, both in the magnitude (asymmetries found in the experiment are larger than in theory) and in the current-dependence. In particular, the increase of the asymmetry with $\langle I_m \rangle$ is in strong contradiction with theory, which predicts a maximum when the shot noise due to the tunnel junction is similar in magnitude to the thermal noise seen at zero current. Two reasons can be invoked for this disagreement: an imperfect modeling of the experiment by theory, or experimental artifacts.

4.1 Effects not considered by theory

The experimental setup presents differences from the simplified circuit described by theory: the RC combination that allows in the experiment to separate low and high frequency fluctuations is not treated by theory; the resistance R_f in series with the tunnel junction also produces noise that modifies the voltage across the tunnel junction, a configuration in which feed-back effects lead to an asymmetry of the current fluctuations [8] that has not been considered; the voltage across the Josephson junction has fluctuations due to plasma oscillations, leading to voltage fluctuations that have been neglected. At least this last point can be discarded, since the corresponding voltages

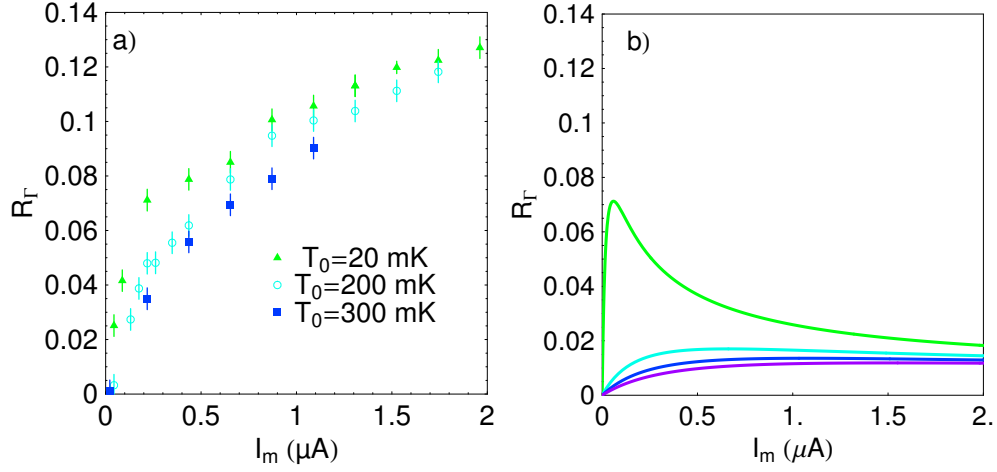


Fig. 8 a) Measured asymmetry R_r as function of the current I_m at a fixed value of the exponent $B = 10.5$ in the rate (1) for various temperature. b) Same quantity calculated using (11), assuming the actual temperature is the refrigerator temperature.

$\approx \varphi_0 \omega_p$ are in the μV range. More work is necessary to analyze the effects of the two other main differences between experiment and theoretical modeling.

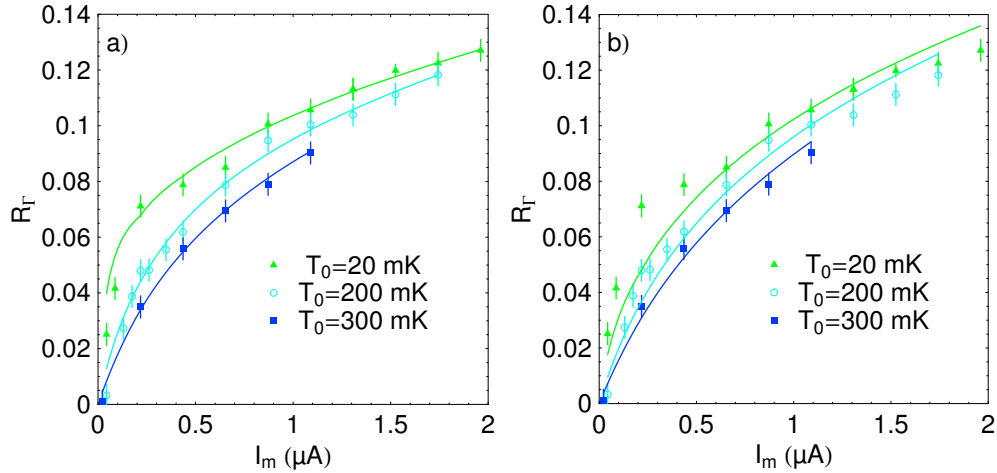


Fig. 9 a) Plot of the asymmetry R_r for a fixed value $B = 10.5$ assuming that the actual value of the current s is given by $s \leftarrow s \pm \lambda \langle I_m \rangle / I_0$ because of a possible leak through the capacitor C_1 . Besides, the temperature θ_{eff} was extracted from Fig.5 instead of being calculated from Eq.(9). Here, $\lambda = 5.5 \times 10^{-4}$ leads to the best fit with the data. b) Same thing assuming that the third moment is 0, that is $g = 0$. Here, $\lambda = 7 \times 10^{-4}$ leads to the best fit with the data.

4.2 Experimental artifact?

We have also explored another possible source of asymmetry associated with an hypothetic imperfection in the experiment, namely a leak across one of the coupling capacitances C or C_1 or a touch to ground of the corresponding bias line. In this case, a fraction λ of the DC current through the junction passes through the Josephson junction instead of returning entirely through the resistor R_f : at $\langle I_m \rangle > 0$, the switching rate at $I_b > 0$ is increased, whereas at $\langle I_m \rangle < 0$ it is decreased. The corresponding asymmetry can be evaluated using Eq. (1) with B evaluated at $s = (I_b \pm \lambda \langle I_m \rangle) / I_0$. For $\lambda \ll 1$, one obtains

$$R_\Gamma \approx 3B(1 - s)^{-1} \lambda \langle I_m \rangle / I_0. \quad (15)$$

The best fit of the data with this expression in which the measured escape temperatures are plugged in, obtained with $\lambda = 7 \times 10^{-4}$, is presented in Fig. 9b. The general trend is well reproduced, but systematic deviations are observed for the data at $T_0 = 20$ mK and at currents above $1 \mu A$. In Fig. 9a, we fitted the data with the conjugated effect of a leak and of the asymmetry expected from the third order cumulant of the current fluctuations (replacing again the effective temperature θ_{eff} by the measured escape temperature). In the best fit, obtained with $\lambda = 5.5 \times 10^{-4}$, all the data are precisely accounted for. If this scenario is the correct one, the asymmetry due to the tunnel junction is clearly seen in the data at the lowest bath temperature, but the uncertainty is too large for other temperatures. The value of λ corresponds to a leak resistance of $R_t / \lambda \approx 3 \text{ M}\Omega$ ($R_f / \lambda \approx 0.4 \text{ M}\Omega$) if the leak comes from the capacitor C_1 (C). The capacitors were tested after fabrication, but a leak might have appeared afterwards. A touch to ground of the corresponding connection line at this intermediate value seems unlikely.

5 Conclusions

In conclusion, we have measured the switching rate of a Josephson junction when coupled to a voltage-biased NIS junction. The main effect is a well explained increase of the escape temperature due to shot noise through the junction. The asymmetry of the rates for opposite signs of the bias of the NIS junction is larger than expected from the dynamics of the Josephson junction in presence of non-Gaussian noise. Part of the discrepancy might be due to an oversimplification in the modelling of the circuit. It is however suspected that a current leak through a capacitor, is responsible for a large fraction of the signal. Experiments less prone to experimental artifacts, with an improved decoupling of the detector from the noise source at DC, are in progress.

A Appendix: Sensitivity of the switching probability to a rate asymmetry

For each current pulse we recorded the boolean 1 or 0 depending whether the voltage across the Josephson junction crossed the threshold or not. The booleans are N independent random variables X_i with binomial distribution, P_{sw} being the expectation for $X_i = 1$. Therefore, the standard deviation of the average $N^{-1} \sum_{i=1}^N X_i$ is $\sqrt{P_{sw}(1 - P_{sw})/N}$. And using

$$P_{sw} = 1 - e^{-\Gamma \tau_p}, \quad (16)$$

one gets the standard deviation of the switching rate

$$\delta\Gamma = \sqrt{\frac{P_{sw}}{N(1 - P_{sw})}} \tau_p^{-1}. \quad (17)$$

Therefore, the uncertainty on the measurement of R_Γ is given by (see Eq. (17)):

$$\delta R_\Gamma = 2 \frac{\delta \Gamma}{\Gamma} = -2 \sqrt{\frac{P_{sw}}{N(1-P_{sw})}} \frac{1}{\ln(1-P_{sw})}. \quad (18)$$

This function presents a minimum at $\delta R_\Gamma \approx 2.5/\sqrt{N}$ for $P_{sw} \approx 0.8$, and grows rapidly near $P_{sw} = 0$ and $P_{sw} = 1$. In the experiment, we chose the range of s so that $0.25 < P_{sw} < 0.987$ (or equivalently $9.3 < B < 12$ in the notations of Eq. (1)) for which $\delta R_\Gamma < 4/\sqrt{N}$, and adapted N at each value of P_{sw} to keep δR_Γ at a fixed value.

Acknowledgements Discussions with Hermann Grabert, Jukka Pekola, Eugene Sukhorukov and within the Quantronics group are gratefully acknowledged. This work was partly funded by the Agence Nationale de la Recherche under contract ANR-05-NANO-039. NB acknowledges partial support by the NSF under grant DMR-0405238. JA acknowledges support from the DFG through the Heisenberg program.

References

- [1] L. Levitov and G. Lesovik, JETP Lett. **55**, 555 (1992).
- [2] Y. Nazarov, Ann. Phys. (Leipzig) **8**, SI (1999).
- [3] W. Belzig and Y. Nazarov, Phys. Rev. Lett. **87**, 197006 (2001).
- [4] K. E. Nagaev, Phys. Rev. B **66**, 075334 (2002).
- [5] S. Pilgram, A. N. Jordan, E. V. Sukhorukov and M. Buttiker, Phys. Rev. Lett. **90**, 206801 (2003).
- [6] B. Reulet, J. Senzier and D. Prober, Phys. Rev. Lett. **91**, 196601 (2003).
- [7] C.W.J. Beenakker, M. Kindermann and Yu.V. Nazarov, Phys. Rev. Lett. **90**, 176802 (2003).
- [8] B. Reulet in *Nanophysics: coherence and transport*, H. Bouchiat, Y. Gefen, S. Guéron, G. Montambaux and J. Dalibard (Eds), p. 361-382, Elsevier (2005).
- [9] Y. Bomze, G. Gershon, D. Shovkun, L. Levitov and M. Reznikov, Phys. Rev. Lett. **95**, 176601 (2005).
- [10] T.T. Heikkilä and T. Ojanen, Phys. Rev. B **75**, 035335 (2007).
- [11] S. Gustavsson, R. Leturcq, B. Simovic, R. Schleser, T. Ihn, P. Studerus, K. Ensslin, D. C. Driscoll and A. C. Gossard, Phys. Rev. Lett. **96**, 076605 (2006).
- [12] T. Fujisawa, T. Hayashi, R. Tomita, and Y. Hirayama, Science **312**, 1634 (2006).
- [13] R.K. Lindell, J. Delahaye, M. A. Sillanpää, T. T. Heikkilä, E. B. Sonin, and P. J. Hakonen, Phys. Rev. Lett. **93**, 197002 (2004).
- [14] J. Tobiska and Yu. V. Nazarov, Phys. Rev. Lett. **93**, 106801 (2004).
- [15] A. V. Timofeev, M. Meschke, J. T. Peltonen, T. T. Heikkilä, and J. P. Pekola, Phys. Rev. Lett. **98**, 207001 (2007).
- [16] A. Barone and G. Paterno, *Physics and Applications of the Josephson Effect* (Wiley, New York, 1982).
- [17] K. K. Likharev, Rev. Mod. Phys. **51**, 101 (1979).
- [18] B. Huard, Ann. Phys. Fr. **31**, N° 4-5 (2006).
- [19] In other experiments, high frequency noise was detected with a Josephson junction biased near the gap. See P.-M. Billangeon, F. Pierre, H. Bouchiat and R. Deblock, Phys. Rev. Lett. **96**, 136804 (2006), and references therein.
- [20] J. P. Pekola, T. E. Nieminen, M. Meschke, J. M. Kivioja, A. O. Niskanen, and J. J. Vartiainen, Phys. Rev. Lett. **95**, 197004 (2005).
- [21] M.H. Devoret, D. Esteve, J.M. Martinis, A. Cleland, and J. Clarke, Phys. Rev. B **36**, 58 (1987).
- [22] B. Huard, H. Pothier and D. Esteve (to be published).
- [23] J. Ankerhold, Phys. Rev. Lett. **98**, 036601 (2007).
- [24] We note that in [23] a factor 2/3 has been forgotten in the definition of the third cumulant. The result for the rate asymmetry given there must thus be multiplied by 2/3 to get (11).
- [25] E.V. Sukhorukov and A.N. Jordan, Phys. Rev. Lett. **98**, 136803 (2007).
- [26] S. Linkwitz, H. Grabert, E. Turbot, D. Esteve and M. H. Devoret, Phys. Rev. B, **45** R3369 (1992).